Journal of Materials Chemistry A

Accepted Manuscript

This article can be cited before page numbers have been issued, to do this please use: Y. Zhan, X. Zhou, H. Nie, X. Xu, X. Zheng, J. Hou, H. Duan, S. Huang and Z. Yang, *J. Mater. Chem. A*, 2019, DOI: 10.1039/C9TA02997D.

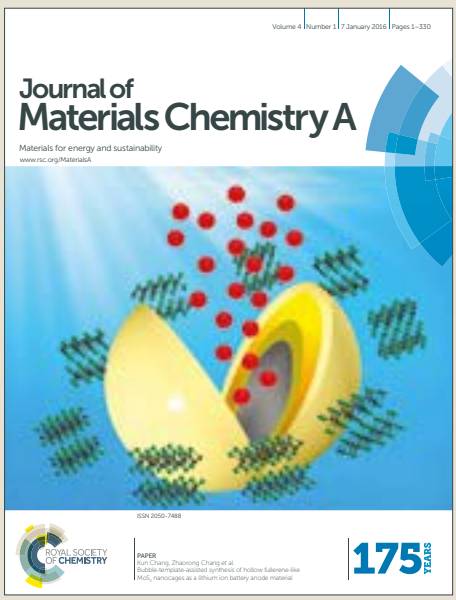

ROYAL SOCIETY OF CHEMISTRY

rsc.li/materials-a

View Article Online
DOI: 10.1039/C9TA02997D

Designing the Pd/O co-doped MoS_x for boosting hydrogen evolution reaction

Yingxin Zhan[+a], Xuemei Zhou[+a, b], Huagui Nie*[a], Xiangju Xu[a], Xiannuo Zheng[a], Junjie Hou[a], Huan Duan[c], Shaoming Huang*[b], Zhi Yang*[a]

Y. Zhan, X. Zhou, H. Nie, X. Xu, X. Zheng, J. Hou, Prof. Z. Yang

[a] Key Laboratory of Carbon Materials of Zhejiang Province, College of Chemistry and Materials Engineering, Wenzhou University, Wenzhou, 325035, PR China

Email: huaguinie@126.com ; yang201079@126.com

X. Zhou, S. Huang

[b] School of Material and Energy, Guangdong University of Technology, Guangzhou, 510006, China

Email: smhuang@wzu.edu.cn

H. Duan

[c] School of Chemistry and Chemical Engineering, Southwest University, Chongqing, 400715, China

[+] These authors contributed equally to this work.

Abstract

Molybdenum disulfide has a great potential as electrocatalyst to drive the hydrogen evolution reaction (HER), but HER catalysts based on transition metal (TM) and non-metal (NM) co-doped MoS_2 have rarely been reported because of the difficulty of preparation. Herein, we design an upgraded sacrificial-counter-electrode method to create a favorable environment for atomic-scale substitution to synthesize Pd/O co-doped MoS_x (Sub-MoS_x/CNTs/Pd_{gly}), which exhibits a small overpotential of 23 mV at a current density of 10 mA cm^{-2}, a low Tafel slope of 18 mv dec^{-1} and good catalytic stability. Density functional theory (DFT) calculations reveal that the Pd/O co-doped MoS_2 tends to form defect-pairs (Pd_{Mo}+O_S) in MoS_2, and the unsaturated S atoms around the defects enormously promote the HER activity.

View Article Online
DOI: 10.1039/C9TA02997D

Introduction

Hydrogen, which is considered promising as a clean energy carrier to replace fossil fuels, can be produced by electrocatalytic water splitting.[1-7] Platinum (Pt) and its alloys remain the first choice among electrocatalysts for the hydrogen evolution reaction (HER) because of their excellent activity and high current density,[8-10] but the use of Pt is limited by its high cost and scarcity in the Earth's crust.[1,11-14] Therefore, the development of low-Pt-loading or Pt-free catalysts with competitive performance remains an important goal.

The free energy of hydrogen adsorption, ΔG_H, for molybdenum disulfide (MoS_2) lies just below those of the noble metals (of which Pt is a member), suggesting the great potential of MoS_2-based materials as an alternative to Pt for the HER.[15] Theoretical studies have predicted that the catalytic activity of MoS_2 could be further increased by doping and/or substitution with heteroatom to reduce the energy of hydrogen adsorption and change the orbital composition of the valence and conduction bands.[16] Recent work has demonstrated that doping MoS_2 with palladium (Pd)[17] or zinc (Zn)[18] could further improve the HER activity of phase-pure MoS_2. In theory, the simultaneous introduction of both transition metal (TM) and non-metal (NM) impurities into the MoS_2 lattice is more energetically favorable than the case of single TM/NM element substitution. Additional NM atoms can cooperate with single-TM-doped MoS_2 to further activate the catalytically inert basal plane of MoS_2. Therefore, the development of co-doped catalysts with high hydrogen evolution activity merits significant attention. However, to the best of our knowledge, HER

View Article Online
DOI: 10.1039/C9TA02997D

catalysts based on TM and NM co-doped MoS_2 have rarely been reported because of the difficulty of preparation. Certain crucial issues must still be resolved: (1) The search for a thermodynamically stable composition for a TM and NM co-doped MoS_2 system. (2) The dynamic creation of a beneficial atomic-scale environment for element exchange, enabling an efficient strategy to achieve dual-element substitution.

As is known, the elements Pd and Mo have similar atomic radii, while O and S atoms have a similar electron configuration to each other. Because of the higher strength of Mo-O bonds compared with Mo-S, the substitutional oxidation of the MoS_2 basal plane is in principle also thermodynamically favorable.[19] Inspired by the above considerations, we chose the elements Pd and O as dopant atoms to systematically study co-doping of MoS_2. Density functional theory (DFT) calculations were carried out to obtain atomic-scale insight into the synergistic effect of Pd and O co-doping (i.e., the formation of defect-pairs). First, the formation energies of Pd single-atom impurities doped at various sites of 1T- and 2H-MoS_2 were calculated, and the results demonstrated a strong tendency for Pd atoms to substitute at Mo sites, with exothermic energies of -1.34 eV and -2.16 eV, respectively, in 1T- and 2H-MoS_2. These results were consistent with data reported previously.[17,19] Then we calculated the formation energy of different kinds of defect-pairs in MoS_2 (as shown in Fig. 1 and the optimized structure shown in Fig. S1). Comparing to the point defect Pd_{Mo}, the relevant energy for formation of sulfur vacancy and oxygen substitution close to the Pd_{Mo} defect (labeled as $Pd_{Mo}+V_S$ and $Pd_{Mo}+O_S$) would drop down to -2.56 eV and -3.68 eV, and induce the rearrangement of electronic charge around the

View Article Online
DOI: 10.1039/C9TA02997D

impurities, which lead to the variation of Pd state, and brought the difference of catalytic activity. For another kind of defect-pairs (labeled as O_S+Pd_{ads}), transition metal (TM) atoms reactive with the primary point defect O_S resulted in stable defect groups which might enhance the deposition and agglomeration, and the further released energy of 1.54 eV originated from the Pd atoms anchoring next to the O_S defect. But the adsorbed Pd atom was not stable enough, tended to bind with more NM/TM atoms and formed a more stabilized PdO_x clusters.

Based on the above description, Pd/O co-doping clearly significantly affects the electronic structure of the neighboring atoms, which can be expected to play an important role in charge redistribution and therefore in boosting the MoS_2 catalytic activity. Thus, synchronized Pd/O co-doping could be an effective strategy to improve the catalytic activity by addition of an appropriate amount of defect-pairs into the MoS_2 basal plane. Our recent work demonstrated that the S atoms in MoS_x could be substituted with O atoms through a sacrificial-counter-electrode method.[20] This implies that the same method can be used to create a favorable environment for atomic-scale substitution to synthesize Pd/O co-doped MoS_x.

Results and discussion

Herein, we design an upgraded sacrificial-counter-electrode method to synthesize Pd/O co-doped MoS_x, as schematically illustrated in Fig. 2a. Firstly, small-sized MoS_x (Sub-MoS_x) clusters on CNTs (denoted as Sub-MoS_x/CNTs) were obtained through a method described in our previous work (Fig. S2).[21] The small size of the MoS_x structures fully exposed the edge S_2^{2-} and Mo sites on the surface, enabling

View Article Online
DOI: 10.1039/C9TA02997D

them to be easily doped by heteroatoms. For comparison, large-sized MoS_x clusters on the surface of CNTs were obtained by the i-t curve process (denoted as i-t/MoS_x/CNTs, Fig. S3), then used for the following parallel experiment. Secondly, glassy carbon electrodes (GCEs) modified with Sub-MoS_x/CNTs were soaked in aqueous H_2SO_4 solutions, and potential cycling was performed using Pd wire as the sacrificial counter electrode in a three-electrode system to synthesize co-doped MoS_x hybrid catalysts (denoted Sub-MoS_x/CNTs/Pd_{gly}). To create a favorable atomic-scale substitution environment, and facilitate Pd substitution on the surface of MoS_x, glycine (Gly) as a complexing agent was added to the H_2SO_4 solutions. Additionally, parallel experiments without Gly were also carried out under the same synthesis conditions, the products of which were labeled as Sub-MoS_x/CNTs/Pd and i-t/MoS_x/CNTs/Pd, respectively. The HER performances of the as-grown catalysts were evaluated using a graphite rod as a counter electrode in a standard three-electrode system and the corresponding experimental results are shown in Fig. S4, Fig. S5 and Table S1 (see Supplementary note 1). It was found that the Sub-MoS_x/CNTs/Pd_{gly} sample showed the highest catalytic current among all the catalysts, so this sample was chosen as the optimal host material for subsequent experiments.

As observed from the transmission electron microscopy (TEM) images and energy-dispersive X-ray (EDX) elemental mappings (Fig. S6 and Fig. S7), small-sized MoS_x (0.8–5 nm) was uniformly grown on the CNTs. The scanning electron microscopy (SEM) (Fig. 2b) and TEM images (Fig. 2c) of the

View Article Online
DOI: 10.1039/C9TA02997D

Sub-MoS_x/CNTs/Pd_{gly} manifest that Pd particles are evenly decorated on the surfaces of the Sub-MoS_x/CNTs. The high-resolution TEM (HRTEM) images in Fig. 2d-e show no obvious lattice fringes, which indicate that the catalyst may have an amorphous structure. These results are also consistent with the SAED data in Fig. S8, which contains blurry rings generated by the Sub-MoS_x/CNTs/Pd_{gly} that imply non perfect ordering of the catalyst, further confirming that the catalyst may display an amorphous structure (see Supplementary note 2). The EDX mapping results further demonstrate that after the potential cycling process, Pd was uniformly distributed over the Sub-MoS_x/CNTs/Pd_{gly} (inset in Fig. 2d and Fig. S9). Moreover, analysis by inductively coupled plasma optical emission spectroscopy (ICP-OES) demonstrated that the Sub-MoS_x/CNTs/Pd_{gly} samples had a 0.63 wt% Pd loading. For comparison, SEM and TEM images display the morphologies of the bare i-t/MoS_x/CNTs (Fig. S10) and the hybrids grown on Sub-MoS_x/CNTs (Fig. S11) and i-t/MoS_x/CNTs (Fig. S12) with or without glycine in the solution. These as-grown hybrids display Pd dendrites and large aggregations of Pd particles on the surface. The Pd loading of i-t-MoS_x/CNTs/Pd_{gly} and i-t-MoS_x/CNTs/Pd were 0.71% and 0.92%, respectively. These observations clearly reveal that the three distinct features of the upgraded sacrificial-counter-electrode method, namely the introduction of small-sized MoS_x with fully exposed sites, the use of Gly as a complexing agent, and the use of Pd as the counter electrode, which facilitate the formation of Pd/O co-doped or metallic Pd/Pd oxide decorated Sub-MoS_x/CNTs/Pd_{gly}.

The chemical composition and valence state of the as-grown samples were

View Article Online
DOI: 10.1039/C9TA02997D

analyzed by X-ray photoelectron spectroscopy (XPS) and the results are presented in Fig. S13 and Fig. 3. Fig. S13 confirms the existence of C, Mo, S, O, N and Pd in the Sub-MoS_x/CNTs/Pd_{gly}, consistent with the EDX mapping results. Compared with the high-resolution Mo 3d peaks of the Sub-MoS_x/CNTs, the Mo 3d peaks of the samples prepared with the upgraded sacrificial-counter-electrode method all shift to lower binding energies (BEs), revealing that the Mo (VI) has been reduced to Mo (IV) (Fig. 3a and Fig. S14a; Supplementary note 3). Fig. 3b shows the Pd 3d peaks and it can be seen that the binding energies of Pd $3d_{5/2}$ are 336.3 and 337.4 eV, which can be assigned to Pd (II) and Pd (IV), respectively. Fig. S14b shows that the Pd $3d_{5/2}$ peaks of Sub-MoS_x/CNTs/Pd_{gly} shift to higher BEs compared with those of the i-t-MoS_x/CNTs/Pd_{gly} samples, indicating that the valence state of Pd is Pd (IV) and Pd (II) in Sub-MoS_x/CNTs/Pd_{gly}, but Pd (II) and Pd (0) in the Pd dendrites in i-t-MoS_x/CNTs/Pd_{gly}, which is consistent with the previous reports.[22-24] This result is also consistent with the HRTEM images (Fig. 2d-e), suggesting that the Sub-MoS_x/CNTs/Pd_{gly} underwent atomic-scale substitution in the upgraded sacrificial-counter-electrode method. Figure 3b also reveals that Pd (IV) is the dominant oxidation state of palladium only at the surface of Sub-MoS_x/CNTs/Pd_{gly} and Sub-MoS_x/CNTs/Pd, while i-t/MoS_x/CNTs/Pd_{gly}, i-t/MoS_x/CNTs/Pd and CNTs/Pd contain Pd (II) surface sites. We speculate that the subnanometric MoS_x particles of Sub-MoS_x/CNTs featuring fully exposed sites are more reactive than the large-size MoS_x clusters in i-t/MoSx/CNTs, thus promoting the formation of higher valence Pd oxides and Pd/O doping into the MoS_x structure during positive-going

View Article Online
DOI: 10.1039/C9TA02997D

potential scans in the repetitive cyclic voltammetry (CV) procedure. The S 2p spectrum in Fig. 3c and Fig. S14c reveals that the S^{2-} ions are gradually transformed into SO_x^{2-},[25, 26] and the O 1s spectra of the Sub-MoS_x/CNTs/Pd_{gly} show a shift towards lower BEs compared with the Sub-MoS_x/CNTs (Fig. S13). These observations imply that some of the S atoms in MoS_x were replaced by O atoms during the potential cycling process. Taken together, the aforementioned XPS results suggest that we successfully obtained the Pd/O co-doped Sub-MoS_x/CNTs/Pd_{gly} by the upgraded sacrificial-counter-electrode method. Additionally, the N 1s spectra of the Sub-MoS_x/CNTs/Pd_{gly} and i-t/MoS_x/CNTs/Pd_{gly} samples in Fig. 3d and Fig. S14d show a shift towards lower BEs compared with the original Gly sample, which may be attributed to the formation of complexes held together by Pd-N bonds (399.6 eV).[27]

To evaluate the HER activities of the various catalysts, the linear sweep voltammetry (LSV) curves of the pristine CNTs, a commercial Pt/C catalyst, Sub-MoS_x/CNTs, Sub-MoS_x/CNTs/Pd and Sub-MoS_x/CNTs/Pd_{gly} electrodes were measured in 0.5 M H_2SO_4 electrolyte using a graphite rod as a counter electrode in a three-electrode configuration, as shown in Fig. 4a. The Sub-MoS_x/CNTs/Pd_{gly} catalyst shows the highest HER activity among all the samples, delivering a current density of 10 mA cm^{-2} while needing an overpotential of only 23 mV, which is significantly better than that of the commercial Pt/C catalyst (34 mV). The corresponding Tafel plots based on the polarization curves are presented in Fig. 4b, in which Sub-MoS_x/CNTs/Pd_{gly} presents a smaller Tafel slope (18 mV dec^{-1}) than that of commercial Pt/C (30 mV dec^{-1}). These results demonstrate that the HER on both the

View Article Online
DOI: 10.1039/C9TA02997D

Sub-MoS_x/CNTs/Pd_{gly} and Pt/C proceeded via the Volmer-Tafel mechanism, with recombination between adjacent adsorbed H atoms as the rate-limiting step (RLS).[20] In fact, the overpotential at the specific current density used here (10 mA cm^{-2}) and the Tafel slope of the Sub-MoS_x/CNTs/Pd_{gly} catalyst are superior to most reported Pd-based catalysts, as presented in Fig. 4c and Table S3, S4 and S5. These results verify that the Sub-MoS_x/CNTs/Pd_{gly} electrode displays efficient kinetics of H_2 evolution. For comparison, the catalytic activity of i-t/MoS_x/CNTs/Pd_{gly} and i-t/MoS_x/CNTs/Pd was also evaluated, as shown in Fig. 4d. It is worth noting that there appear hydrogen adsorption peaks for these two samples. By inspection of the SEM and TEM images in Fig. S12, we speculate that these hydrogen adsorption peaks (the inset in Fig. 4d) may be attributed to the formation of Pd dendrites in the i-t/MoS_x/CNTs/Pd_{gly} and i-t/MoS_x/CNTs/Pd samples.[28,29] The hydrogen adsorption peak of i-t/MoS_x/CNTs/Pd_{gly} was lower than that of the i-t/MoS_x/CNTs/Pd electrode (the inset in Fig. 4d). These results, combined with the morphological analysis of the samples (Fig. S12), suggest that Gly isolates the Pd ions through complexation to prevent the large aggregation of Pd particles, which is consistent with the XPS evidence for the formation of Pd-N complexes. These results further demonstrate that the excellent HER catalytic activities of Sub-MoS_x/CNTs/Pd_{gly} originate from the effects of co-doping with Pd and O atoms.

The stability of the catalyst is also an important factor with regard to the HER. Therefore, the stability of the Sub-MoS_x/CNTs/Pd_{gly} and i-t/MoS_x/CNTs/Pd_{gly} electrodes was evaluated by monitoring the current density during continuous

View Article Online
DOI: 10.1039/C9TA02997D

operation at 0.2 V (vs. reversible hydrogen electrode (RHE)) under acidic conditions (Fig. 4e). Significantly, the Sub-MoS_x/CNTs/Pd_{gly} electrode maintained a constant cathodic current for over 24 h with no obvious change. The morphology and structure of Sub-MoS_x/CNTs/Pd_{gly} electrodes after 24 h stability test are shown in Fig. S15 and Fig. S16. From the SEM observations (Fig. S15) and the XPS results (Fig. S16), it is found that the morphology of Sub-MoS_x/CNTs/Pd_{gly} has no obvious change and the catalysts after stability test still maintain the same chemical states. The stability of Sub-MoS_x/CNTs/Pd_{gly} also was tested by cycling the potential for 1000 times between -0.2 and +0.3 V vs. RHE, as given in Fig. S17. The polarization curve of the Sub-MoS_x/CNTs/Pd_{gly} catalyst after 1000 times test is almost identical to the initial one, suggesting negligible loss of cathodic current. This in turn indicates that the Sub-MoS_x/CNTs/Pd_{gly} catalyst exhibits excellent durability under acidic conditions. This level of durability is much greater than those of the majority of previously reported Pd hybrid catalysts (Table S5). Fig. S18 reveals the Faradic efficiency (FE) of Sub-MoS_x/CNTs/Pd_{gly} for water electrolysis by comparing the amount of experimentally measured with theoretically calculated H_2. The amount of H_2 increases during electrolysis process and the approximate agreement of measured value and theoretical one suggests nearly 100% FE.

The electrochemical surface area (ECSA) values were also evaluated to gain further insights into these electrocatalysts. These values were obtained by calculating the electrochemical double layer capacitances (C_{dl}) by simple CV, and the standard CV curves acquired for the different materials with varying scan rates are shown in

View Article Online
DOI: 10.1039/C9TA02997D

Fig. S19. Here, a larger C_{dl} value implies a higher ECSA. As shown in Fig. 4f, the C_{dl} of the Sub-MoS_x/CNTs/Pd_{gly} was approximately 32.3 mF cm^{-2}, much higher than those for the Sub-MoS_x/CNTs/Pd (29.1 mF cm^{-2}), i-t/MoS_x/CNTs/Pd_{gly} (24.5 mF cm^{-2}) and i-t/MoS_x/CNTs/Pd (8.72 mF cm^{-2}), which indicated that the Sub-MoS_x/CNTs/Pd_{gly} hybrid catalyst possessed a larger ECSA. This result further confirmed the successful synthesis of the Pd/O co-doped Sub-MoS_x/CNTs/Pd_{gly} catalyst, in which the small particle size exposed more active sites than in i-t/MoS_x, and Gly functioned as the complexing agent. This resulted in the enhanced HER performance of the Sub-MoS_x/CNTs/Pd_{gly} catalyst through its rapid surface charge transfer, high reaction rate and large ECSA.

The chemical state of Pd in the Sub-MoS_x/CNTs/Pd_{gly}, Sub-MoS_x/CNTs/Pd, i-t/MoS_x/CNTs/Pd_{gly} and i-t/MoS_x/CNTs/Pd catalysts under working conditions were further investigated by CV. We performed CV measurements between 0.05 and 1.2 V vs. RHE in 0.5 M H_2SO_4 on the as-obtained catalysts and those subjected to the HER at a current density of 20 mA cm^{-2} for about 30 minutes. Fig. S20 describe the CVs recorded before and after the HER treatment, which reveals the appearance or augmentation of anodic voltammetric peaks near 0 V vs. RHE (sharp or broad) after the HER treatment. These peaks can be readily assigned to oxidation of hydrogen absorbed in the metallic Pd lattice, which suggests that Pd oxide clusters are partially reduced to Pd (0) under the HER.

In order to elucidate the influence of MoS_x on the structure and HER activity of MoS_x/CNTs/Pd hybrids, we employed the sacrificial-counter-electrode method to

View Article Online
DOI: 10.1039/C9TA02997D

deposit Pd particles directly on CNTs in the presence and absence of glycine in the solution. Fig. S21 shows the SEM images of the CNTs/Pd_{gly} and CNTs/Pd. It can be seen that it tends to form palladium clusters without glycine in the solution. XPS spectra display that the chemical composition and valence state of the CNTs/Pd_{gly} and CNTs/Pd catalysts have no obvious difference, as given in Fig. S22. As given in Fig. S23, it shows that the HER performance of CNTs/Pd_{gly} is better than that of CNTs/Pd catalysts due to CNTs/Pd_{gly} electrodes with high capacitance. However, the HER performance of CNTs/Pd_{gly} is lower than that of Sub-MoS_x/CNTs/Pd_{gly} catalysts, which indicates that the Sub-MoS_x plays an important role in influence the HER activity of Sub-MoS_x/CNTs/Pd_{gly} catalysts. Fig. S21 proves that Pd particles/clusters are formed even on bare CNTs (without MoS_x) during the CV procedure, as in the cases when the Sub-MoS_x/CNTs and i-t/MoS_x/CNTs substrates are applied (Figs. 2, S11 and S12). These results of XPS (Fig. 3b), CV (Fig. S20) and SAED (Fig. S8) suggest that all these Pd deposits consist of metallic Pd covered with Pd oxide layers.

With reference to the above results, it cannot be claimed that Pd/O doping into MoS_x predominantly or exclusively occurs during the repetitive potential cycling synthesis of Sub-MoS_x/CNTs/Pd_{gly} or Sub-MoS_x/CNTs/Pd, but the procedure also leads to the direct deposition of Pd particles on the surface of the MoS_x and CNTs of Sub-MoS_x/CNTs in the presence of glycine. It is reasonable to conclude that the CV synthesis method of Sub-MoS_x/CNTs/Pd_{gly} and Sub-MoS_x/CNTs/Pd results in both Pd/O co-doping into MoS_x and metallic Pd/Pd oxides formation. The significant difference in HER activity between Sub-MoS_x/CNTs/Pd_{gly} and Sub-MoS_x/CNTs/Pd

View Article Online
DOI: 10.1039/C9TA02997D

may be attributed that, with the help of glycine, more Pd/O doping sites occurred on the surface of Sub-MoS_x/CNTs/Pd_{gly} than Sub-MoS_x/CNTs/Pd. Although Pd/O doping also occurs in Sub-MoS_x/CNTs/Pd, without the help of glycine, the Pd ion migration rate is fast, making it easier to form metal Pd/Pd oxides on the surface, which eventually leads to the increase of Pd content (Table S2) on the surface, reducing the interface area between electrode and electrolyte and reducing the activity.

To further investigate the atomic-scale doping effect of Pd and O on the Sub-MoS_x/CNTs/Pd_{gly} catalytic system, DFT calculations were carried out to explore the influence of defect-pairs on the HER performance of both the 1T- and 2H-MoS_2, as evaluated by the ΔG_H values. A ΔG_H value of approximately zero would imply excellent catalytic performance.[30] Fig. 5 shows the adsorption structures of hydrogen on the 1T- and 2H-MoS_2 containing defect-pairs (Pd_{Mo}+O_S), illustrated by the top and front views of the optimized models, and a diagram of the ΔG_H energy levels of the active catalytic sites of the doped system. Evidently, the S atoms on the pure MoS_2 surface were inert to H adsorption, with a highly positive ΔG_H value of 2.11 eV, agreeing with the data in previous reports. [19,20,30] For Pd_{Mo}+O_S defect pairs, the Pd top site was also calculated to be inactive for adsorption, as H atoms were more inclined to bind with the neighboring NM atoms near the defect-pairs through sharing a pair of electrons. However, the calculated ΔG_H at the S1 sites, which were located close to the Pd_{Mo}+O_S defects, dropped dramatically by 1.98 eV compared with adsorption on the S of pure MoS_2. This suggests that these unsaturated S atoms could be activated

View Article Online
DOI: 10.1039/C9TA02997D

by the defect-pairs, comparable to the mechanism of Pt catalysts. Moreover, the doped O atoms also behaved as new active sites with the value of ΔG_H = -0.24 eV. For O_S+PdO cluster (Fig. S24), since the ionization energy of Mo was less than that of Pd, and the electronegativity of O was more than that of S, Pd atom adjacent O_S defect received more electrons from the adjacent O and two S atoms with more 4d-states filled, which lead to a weaker interaction with H atoms than bulk Pd phase, obtaining the value of ΔG_H = -0.12 eV. Comparing the ΔG_H values of the two different structures (1T and 2H) of MoS_2, the 1T-MoS_2 containing Pd_{Mo}+O_S defects showed better HER catalytic behavior than that of the 2H-MoS_2 basal plane. These calculated results indicate that the Pd/O co-doping and the unsaturated S atoms around the defects would enormously promote the HER activity, concurring with our experimental observations that the HER performance was greatly enhanced by the presence of 0.63% defect-pairs in MoS_2. Based on the calculated and experimental results, we inferred that the significant increase in the catalytic activity was caused by the Pd_{Mo}+O_S defect-pairs and/or PdO clusters.

Conclusions

In summary, we have successfully synthesized Pd/O co-doped Sub-MoS_x/CNTs/Pd_{gly} via an upgraded sacrificial-counter-electrode method. This catalyst with ultra-low Pd loading (0.63 wt%) exhibits an excellent HER performance, with a small overpotential of 23 mV at a current density of 10 mA cm^{-2}, a low Tafel slope of 18 mv dec^{-1} and good catalytic stability. The HER activity of Sub-MoS_x/CNTs/Pd_{gly} is comparable to or even better than that of Pt/C in acidic solutions. DFT calculations

View Article Online
DOI: 10.1039/C9TA02997D

indicate that the Pd/O co-doping and the unsaturated S atoms around the defects enormously promote the HER activity. Therefore, this study opens up a new avenue for developing highly efficient co-doped catalysts for hydrogen production, leading to a promising future in replacing Pt-based electrocatalysts for the HER. It can also be anticipated that this strategy can be extended to wider catalyst applications such as O_2 and N_2 reduction.

Acknowledgements

The work was supported in part by grants from National Natural Science Foundation of China (21875166, 51741207, 51572197, 21475096) and Natural Science Foundation of Zhejiang Province for Distinguished Young Scholars (LR18E020001).We are grateful to ShenZhen Jiabin Tech. Co. Ltd. for scientific computing assistance. We thank Michael D. Judge, from Liwen Bianji, Edanz Editing China for editing the English text of a draft of this manuscript.

Notes and references

1 X. Zou and Y. Zhang, *Chem. Soc. Rev.*, 2015, **44**, 5148-5180.

2 C. G. Morales-Guio, L. A. Stern and X. Hu, *Chem. Soc. Rev.*, 2014, **43**, 6555-6569.

3 R. Wu, B. Xiao, Q. Gao, Y.-R. Zheng, X.-S. Zheng, J.-F. Zhu, M.-R. Gao and S.-H. Yu, *Angew. Chem. Int. Ed.*, 2018, **57**, 15445-15449.

4 H. Wu, X. Lu, G. Zheng and G. W. Ho, *Adv. Energy Mater.*, 2018, **8**, 1702704.

5 F. Li, G. F. Han, H. J. Noh, Y. Lu, J. Xu, Y. Bu, Z. Fu and J. B. Baek, *Angew. Chem. Int. Ed.*, 2018, **57**, 14139-14143.

6 Y. Dong, S. Zheng, J. Qin, X. Zhao, H. Shi, X. Wang, J. Chen and Z. S. Wu, *ACS nano*, 2018, **12**, 2381-2388.

7 Z. Xiao, Y. Wang, Y.-C. Huang, Z. Wei, C.-L. Dong, J. Ma, S. Shen, Y. Li and S. Wang, *Energy Environ. Sci.*, 2017, **10**, 2563-2569.

8 L. Cao, Q. Luo, W. Liu, Y. Lin, X. Liu, Y. Cao, W. Zhang, Y. Wu, J. Yang, T. Yao and S. Wei, *Nat. Catal.*, 2018,**18**, 2520.

9 L. Zhang, L. Han, H. Liu, X. Liu and J. Luo, *Angew. Chem. Int. Ed.*, 2017,**56**, 13694.

10 X. Cheng, Y. Li, L. Zheng, Y. Yan, Y. Zhang, G. Chen, S. Sun and J. Zhang, *Energy Environ. Sci.*, 2017, **10**, 2450-2458.

11 J. Feng, F. Lv, W. Zhang, P. Li, K. Wang, C. Yang, B. Wang, Y. Yang, J. Zhou, F. Lin, G. C. Wang and S. Guo, *Adv. Mater*, 2017, **29**, 1703798.

12 X. Zhu, C. Tang, H.-F. Wang, B.-Q. Li, Q. Zhang, C. Li, C. Yang and F. Wei, *J. Mater. Chem. A*, 2016, **4**, 7245-7250.

13 J. Staszak-Jirkovsky, C. D. Malliakas, P. P. Lopes, N. Danilovic, S. S. Kota, K. C. Chang, B. Genorio, D. Strmcnik, V. R. Stamenkovic, M. G. Kanatzidis and N. M. Markovic, *Nat. Mater*, 2016, **15**, 197-203.

14 J. Shen, Z. Yang, M. Ge, P. Li, H. Nie, Q. Cai, C. Gu, K. Yang and S. Huang, *ACS. Appl. Mater. Interfaces*, 2016, **8**, 17284-17291.

15 Y. Yan, B. Xia, Z. Xu and X. Wang, *ACS. Catal.*, 2014, **4**, 1693-1705.

16 Y. Zheng, Y. Jiao, M. Jaroniec and S. Z. Qiao, *Angew. Chem. Int. Ed.*, 2015, **54**, 52-65.

17 Z. Luo, Y. Ouyang, H. Zhang, M. Xiao, J. Ge, Z. Jiang, J. Wang, D. Tang, X. Cao, C. Liu and W. Xing, *Nat. Commun*, 2018, **9**, 2120.

18 W. Wu, C. Niu, C. Wei, Y. Jia, C. Li and Q. Xu, *Angew. Chem. Int. Ed.*, 2019,**58**,1-6.

19 J. Pető, T. Ollár, P. Vancsó, Z. I. Popov, G. Z. Magda, G. Dobrik, C. Hwang, P. B. Sorokin and L. Tapasztó, *Nat. Chem.*, 2018, **10**, 1246-1251.

20 Y. Zhan, Y. Li, Z. Yang, X. Wu, M. Ge, X. Zhou, J. Hou, X. Zheng, Y. Lai, R. Pang, H. Duan, X. a. Chen, H. Nie and S. Huang, *Adv. Sci.*, 2019, 1801663.

21 P. Li, Z. Yang, J. Shen, H. Nie, Q. Cai, L. Li, M. Ge, C. Gu, X. Chen, K. Yang, L. Zhang, Y. Chen and S. Huang, *ACS. Appl. Mater. Interfaces.*, 2016, **8**, 3543-3550.

22 X.-L. Liang, X. Dong, G.-D. Lin and H.-B. Zhang, *Appl. Catal. B-Environ.*, 2009, **88**, 315-322.

23 D. Gao, C. Zhang, S. Wang, Z. Yuan and S. Wang, *Catal. Commun.*, 2008, **9**, 2583-2587.

24 M. Moroseac, T. Skála, K. Veltruská, V. Matolín and I. Matolínová, *Surf. Sci.*, 2004, **566**, 1118-1123.

25 T. Wang, J. Zhuo, K. Du, B. Chen, Z. Zhu, Y. Shao, M. Li, Adv. Mater., 2014, **26**, 3761.

26 J. Yang, Z.Yang, L. Li, Q. Cai, H. Nie, M. Ge, X. Chen , Y. Chen and S. Huang, Nanoscale, 2017, **9**, 6886-6894.

27 Y.-Y. Liu, H.-P. Zhang, B. Zhu, H.-W. Zhang, L.-D. Fan, X.-Y. Chai, Q.-L. Zhang, J.-H. Liu and C.-X. He, *Electrochim. Acta*, 2018, **283**, 221-227.

28 T. Li, Z. Tang, K. Wang, W. Wu, S. Chen and C. Wang, *Internat. J. Hydrogen Energ.*, 2018, **43**, 4932-4941.

29 A. Safavi, S. H. Kazemi and H. Kazemi, *Fuel*, 2014, **118**, 156-162.

30 H. Li, C. Tsai, A. L. Koh, L. Cai, A. W. Contryman, A. H. Fragapane, J. Zhao, H. S. Han, H. C. Manoharan, F. Abild-Pedersen, J. K. Norskov and X. Zheng, *Nat. Mater*, 2016, **15**, 364.

View Article Online
DOI: 10.1039/C9TA02997D

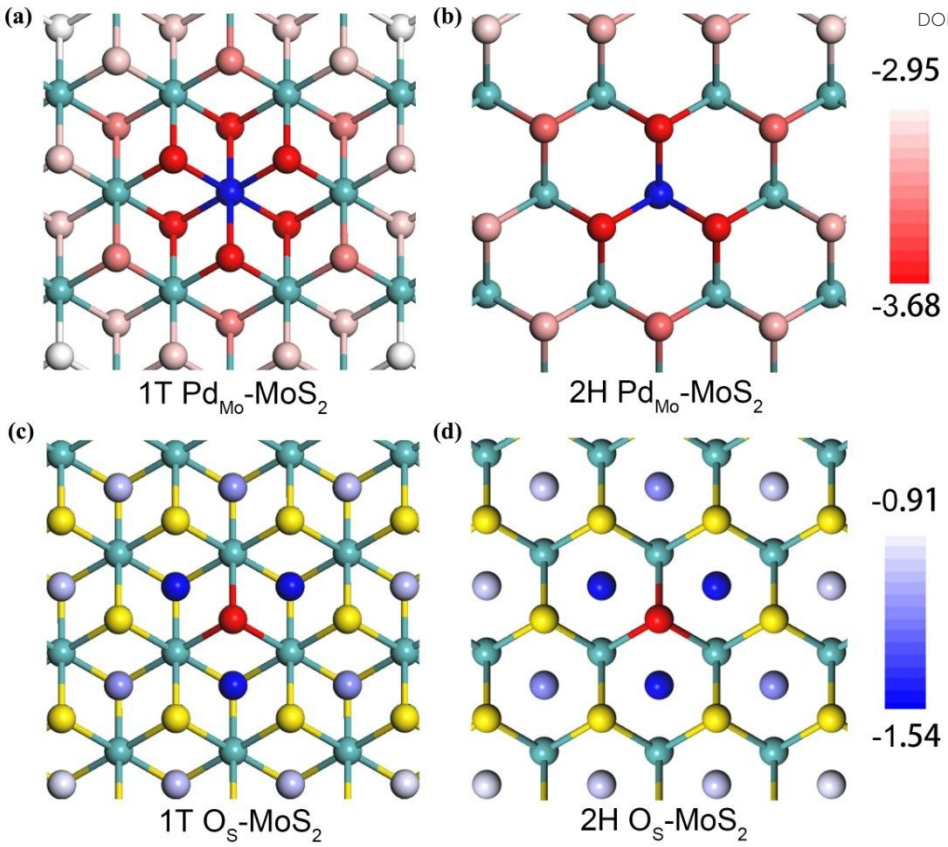

Fig. 1 Formation energy analysis of the defect-pairs in MoS_2 revealing the co-doping nature. The first row represents that O atom substitutes for the S atom at different sites of 1T/2H Pd_{Mo}-MoS_2 with red to white gradient, and the second one contains that Pd atom adsorbs at different sites of 1T/2H O_S-MoS_2 with blue to white gradient. The blue, olivine, yellow and red balls are Pd, Mo, S and O atoms, respectively.

View Article Online
DOI: 10.1039/C9TA02997D

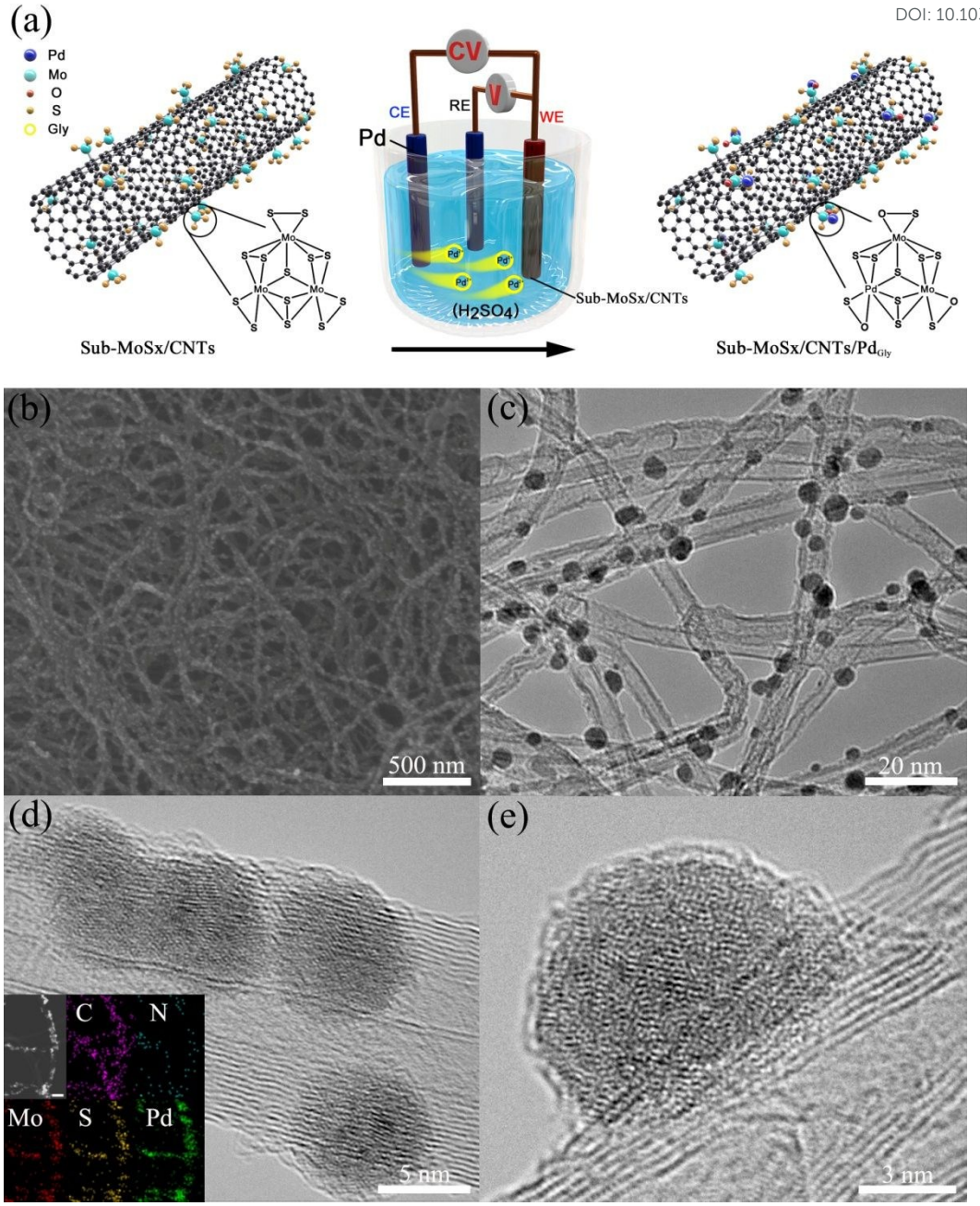

Fig. 2 (a) Schematic illustration of the Sub-MoS_x/CNTs/Pd_{gly} synthesis procedure; Characterizations of the Sub-MoS_x/CNTs/Pd_{gly} hybrid catalysts: (b) SEM image, (c)TEM image, (d) and (e) HRTEM images, the inset shows EDX element maps (scale bar = 200 nm).

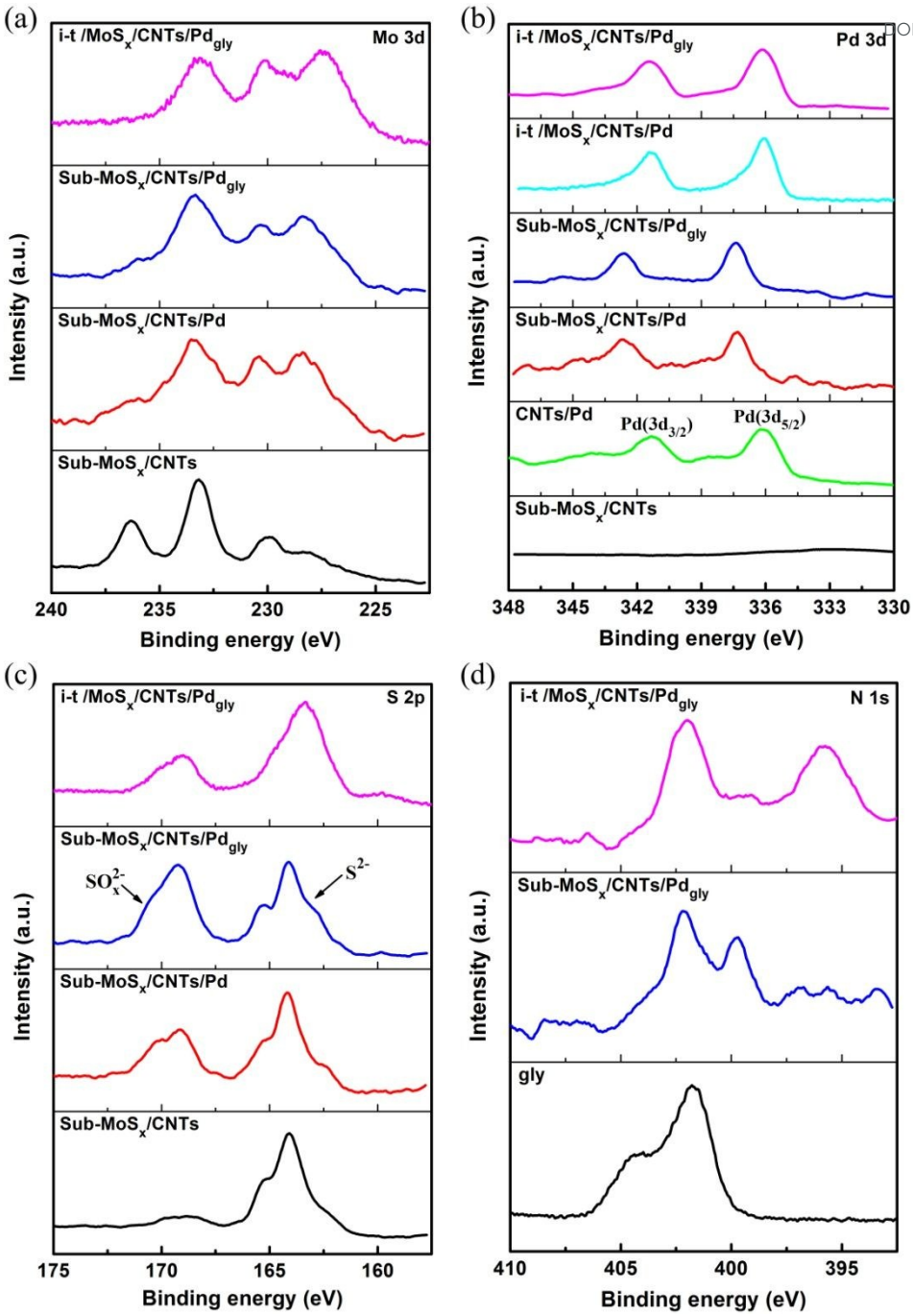

Fig. 3 Structural characterizations of the catalysts: (a) Mo 3d, (b) Pd 3d, (c) S 2p and (d) N 1s spectra of the hybrid catalysts.

View Article Online
DOI: 10.1039/C9TA02997D

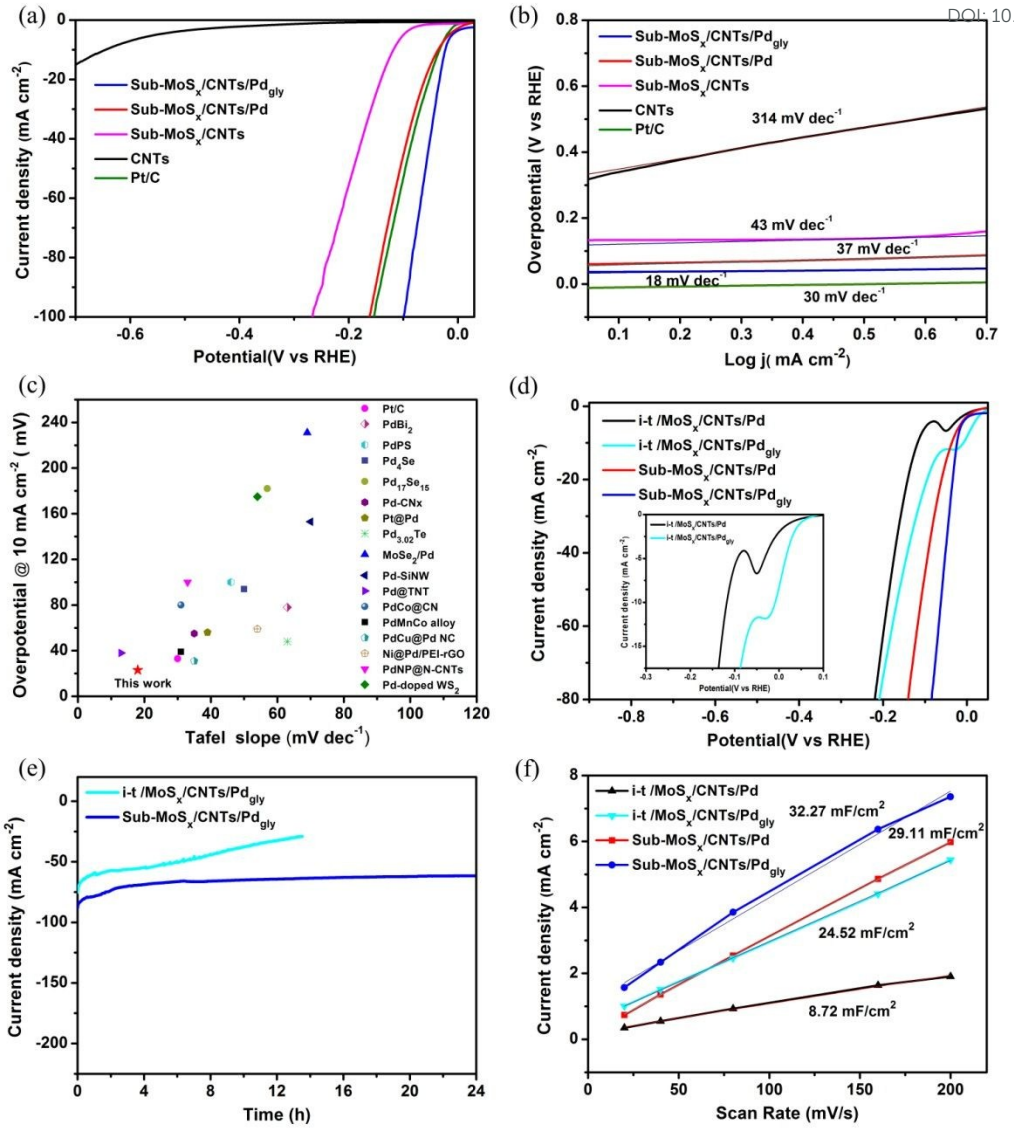

Fig. 4 The HER performance of the catalysts: (a) The polarization curves for CNTs, Pt/C, Sub-MoS_x/CNTs, Sub-MoS_x/CNTs/Pd, and Sub-MoS_x/CNTs/Pd_{gly} in a 0.5 M H_2SO_4 solution at a scan rate of 5 mV s^{-1} and (b) the corresponding Tafel plots. (c) A comparison of the overpotentials at a current density of 10 mA cm^{-2} and the Tafel slopes for the various palladium-based catalysts. (d) The polarization curves for Sub-MoS_x/CNTs/Pd, Sub-MoS_x/CNTs/Pd_{gly}, i-t /MoS_x/CNTs/Pd, and i-t /MoS_x/CNTs/Pd_{gly} in a 0.5 M H_2SO_4 solution at a scan rate of 5 mV s^{-1}. (e) The chronoamperometry i-t curve for Sub-MoS_x/CNTs/Pd_{gly} and i-t /MoS_x/CNTs/Pd_{gly} at η = 200 mV in 0.5 M H_2SO_4. (f) The corresponding double-layer capacitance values of the Sub-MoS_x/CNTs/Pd, Sub-MoS_x/CNTs/Pd_{gly}, i-t /MoS_x/CNTs/Pd, and i-t /MoS_x/CNTs/Pd_{gly} hybrid catalysts.

View Article Online
DOI: 10.1039/C9TA02997D

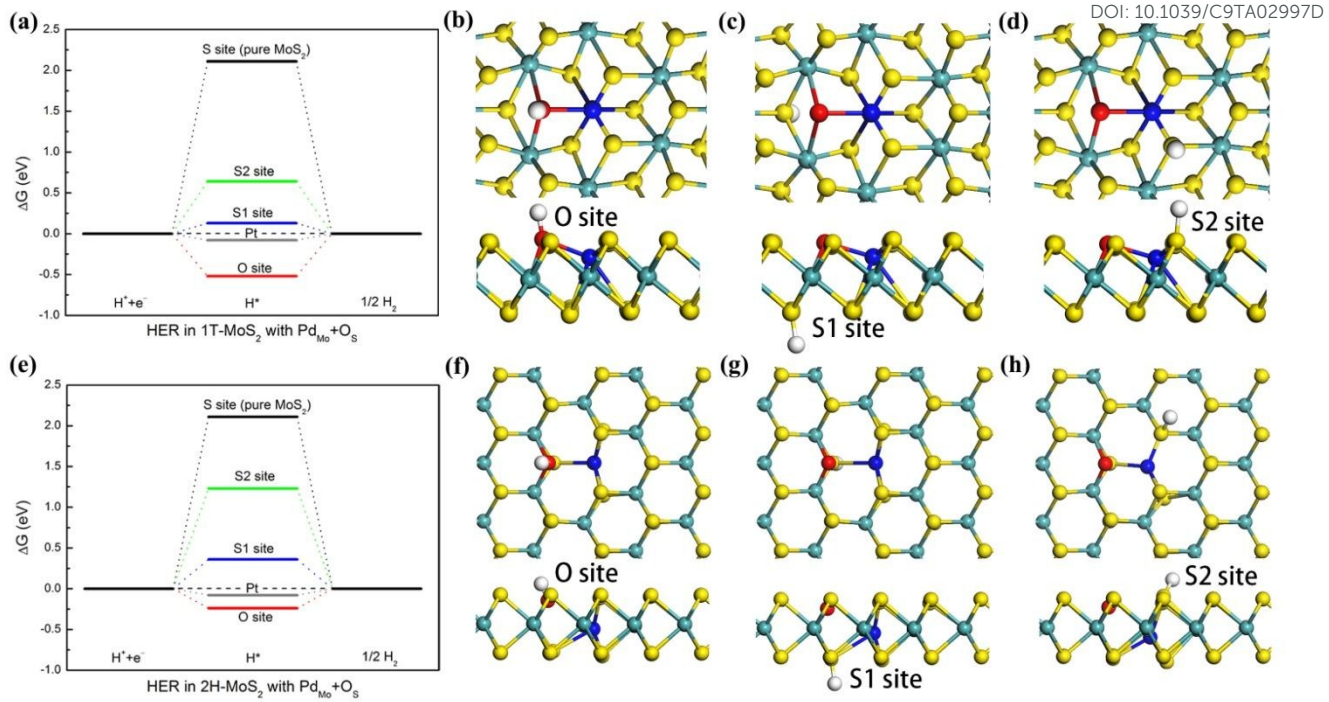

Fig. 5 Binding configurations for single H atom at different adsorbed sites around the Pd_{Mo}+O_S defect-pairs in 1T-MoS_2 and 2H-MoS_2 basal plane, and the Gibbs free energies diagram were given. The blue, olivine, yellow white and red balls were Pd, Mo, S, H and O atoms, respectively.

View Article Online
DOI: 10.1039/C9TA02997D

The table of contents

We introduce a new and original concept involving the transition metal (TM) and non-metal (NM) co-doped MoS_2, and develop an upgraded sacrificial-counter-electrode method to create a favorable environment for atomic-scale substitution to synthesize Pd/O co-doped MoS_x. This catalyst with ultra-low Pd loading (0.63 wt%) exhibits an excellent HER performance, with a small overpotential of 23 mV at a current density of 10 mA cm^{-2}, a low Tafel slope of 18 mv dec^{-1} and good catalytic stability. DFT calculations and experimental results confirm that the Pd/O co-doping and the unsaturated S atoms around the defects (Pd_{Mo}+O_S) would enormously promote the HER activity.